Supplementary information

Poly-Thymine-Mediated Fluorescence Recovery of N-CQDs for Turn-On Sensing of APE1 Activity in Breast Cancer Cell Lysates

Xinjuan Xiong[1], Yanning Li[1], Minghui Zhao[1], Juan Zhao[1], Shulong Xiong[2], Zhao Sun[1]*

[1] Department of Thyroid and Breast Surgery, The 960th Hospital of the PLA Joint Logistics Support Force, Jinan, 250031, China.

[2] Hunan Academy of Chinese Medicine, Changsha, 410208, China.

Corresponding Author: Zhao Sun

Email: sunzhao1022@163.com

Materials and Reagents

Silver nitrate ($AgNO_3$) and other metal salts (NaCl, KCl, $MgCl_2$, $CaCl_2$, $ZnCl_2$, $CuCl_2$, $FeCl_3$) were purchased from Sigma-Aldrich. Fetal bovine serum (FBS) and cell culture media were from Gibco. All enzymes-including Apurinic/apyrimidinic endonuclease 1 (APE1), DNase I, Exonuclease III, Endonuclease IV, Alkaline Phosphatase (ALP), and Trypsin-as well as Bovine Serum Albumin (BSA) were sourced from New England Biolabs. The DNA probes T1 and T2 were synthesized and HPLC-purified by Sangon Biotech (Shanghai). Tris-HCl buffer, and RIPA lysis buffer were obtained from Thermo Fisher Scientific. All solutions were prepared using deionized water (18.2 MΩ·cm, Milli-Q).

Instrumentation

The UV absorption and fluorescence spectra were recorded using a UV-1800 UV-vis spectrophotometer (Shimadzu, Japan) and a FL-2500 Fluorescent Photometer (Hitachi, Japan), respectively. N-CQDs was characterized using high resolution transmission electron microscopy (HR-TEM) at an accelerating voltage of 200 kV (JEOL Co., Japan). Energy-dispersive X-ray spectroscopy (EDS) analysis of N-CQDs was performed using a JEM-F200 TEM at an accelerating voltage of 200 kV (JEOL Co., Japan). X-ray photoelectron spectroscopy (XPS) images of N-CQDs and Ag^+ + N-CQDs were obtained using an AXIS SUPRA+ spectrometer (Shimadzu, UK). Sample preparation was carried out using a constant temperature oscillating metal bath incubator (MB-102, Hangzhou, China).

Synthesis of N-CQDs

N-doped carbon quantum dots (N-CQDs) were synthesized via a one-pot hydrothermal method. Briefly, 2.0 g of washed and dried castor seeds were ground into powder, dispersed in 30 mL deionized water, and sonicated to form a homogeneous suspension. The mixture was transferred into a Teflon-lined autoclave and heated at 180 °C for 10 h. After cooling, the resulting solution was centrifuged and filtered through a 0.22 μm membrane. The filtrate was dialyzed (MWCO: 1000 Da) against water for 48 h to remove small molecules. The purified N-CQDs solution was stored at 4 °C for further use.

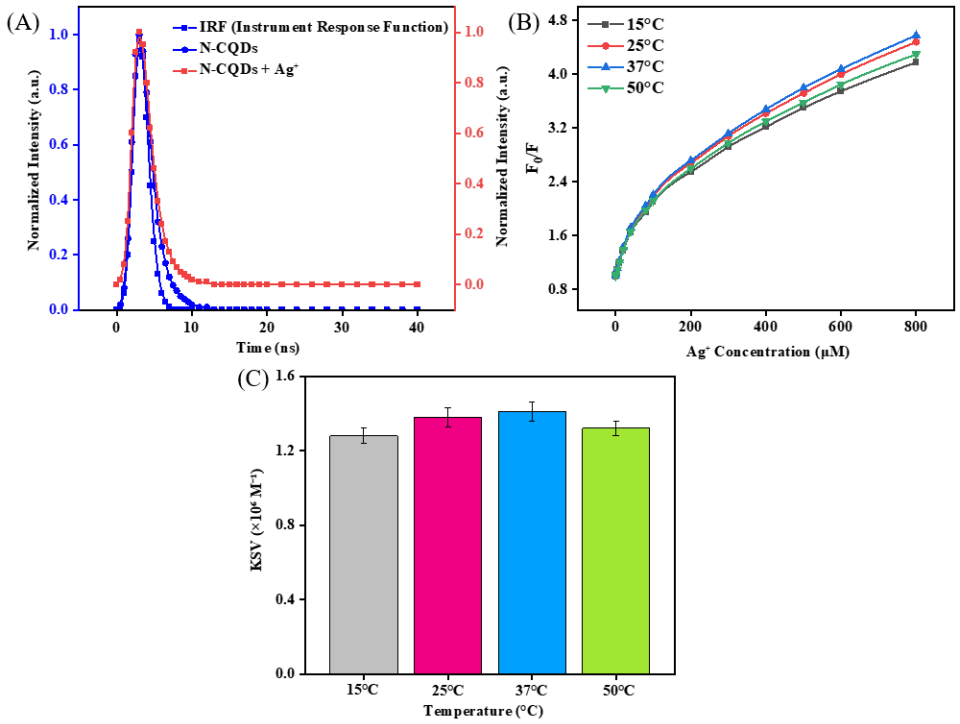

Figure S1. Mechanistic investigation of the inner filter effect (IFE). (A) Time-resolved fluorescence decay curves of N-CQDs in the absence (blue) and presence (red) of Ag^+. The instrument response function (IRF, gray dashed line) is shown for reference. The average fluorescence lifetimes were determined to be 6.42 ± 0.15 ns for N-CQDs alone and 6.38 ± 0.18 ns for N-CQDs with Ag^+. No significant change in lifetime was observed, supporting the IFE mechanism. (B) Stern-Volmer plots of N-CQDs quenched by Ag^+ at different temperatures (15, 25, 37, and 50 °C). (C) Corresponding Stern-Volmer quenching constants (K_SV) at different temperatures. The K_SV values remained relatively stable across the temperature range (1.28-1.41 × 10^6 M^{-1}), showing no significant temperature-dependent increase or decrease, which is characteristic of the IFE.

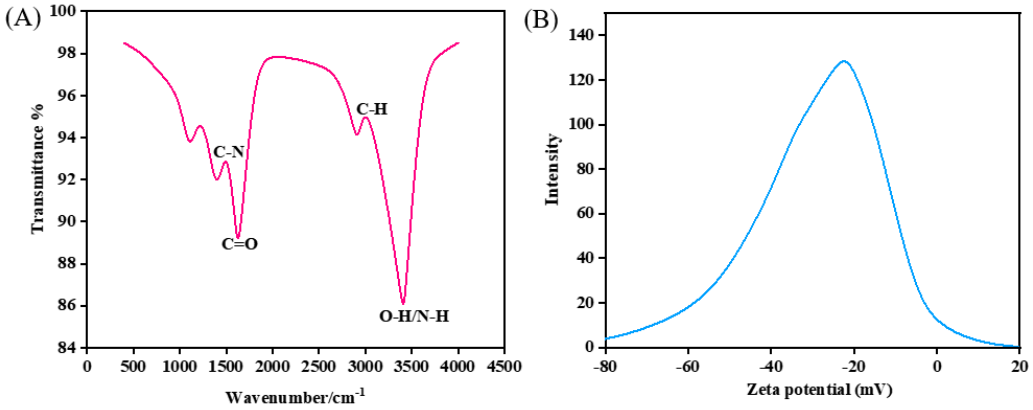

Figure S2. (A) FTIR spectrum of N-CQDs. Characteristic peaks at 3420 cm^{-1} (O-H/N-H stretching), 1635 cm^{-1} (C=O stretching), 1402 cm^{-1} (C-N stretching), confirm the surface functional groups. (B) Zeta potential distribution of N-CQDs in water, showing a mean value of-22.4 ± 3.1 mV.

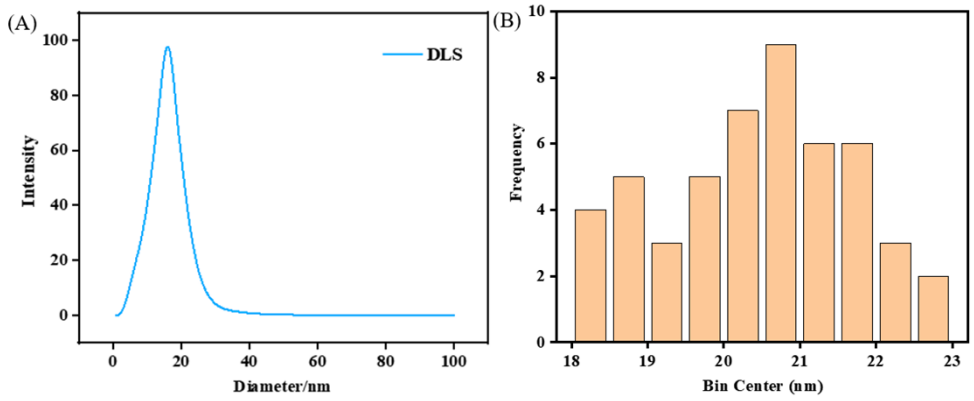

Figure S3. (A) Dynamic light scattering (DLS) intensity-weighted size distribution of N-CQDs in water, showing a mean hydrodynamic diameter of 15.8 nm (PDI = 0.18). (B) Size distribution histogram of N-CQDs obtained from TEM images (n = 50), giving an average diameter of 20.1 ± 1.2 nm. The results confirm the nanoscale size and good monodispersity of the N-CQDs.

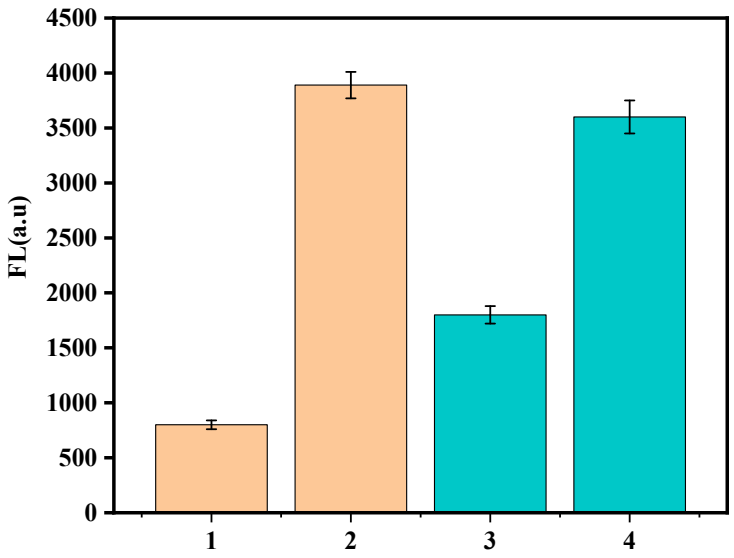

Figure S4. Effect of magnetic beads (MB) on the fluorescence response of the biosensor. Four conditions were compared: (1) MB + no APE1-probe immobilized on magnetic beads, no APE1 added (background control); (2) MB + APE1-probe on beads with APE1 (signal); (3) No MB + no APE1- free probe in solution without APE1 (background without MB); (4) No MB + APE1-free probe with APE1 (signal without MB). Fluorescence intensities were measured at 450 nm. Data are presented as mean ± SD (n = 3). The signal-to-background ratios were 4.86 (3890/800) for the MB-assisted system and 2.00 (3600/1800) without MB. The use of MBs significantly reduced background fluorescence (800 vs. 1800) and provided a clear "OFF-to-ON" response. Without MBs, the high background and poor signal-to-background ratio would lead to false-positive results, demonstrating that MBs are essential for reliable APE1 detection.

Table S1. DNA sequences (5′-3′) utilized in this work. (X represent AP site).

Strand	Sequence (5′-3′)
T1	Biotin-CAGTCACTCGATCCAATCTACAGC
T2	TTGGATCGAXT$_{(30)}$

Table S2. Recovery of APE1 in fetal bovine serum (FBS)

Spiked (U/mL)	Found (U/mL)	Recovery (%)	RSD (%) (n=3)
0.06	0.058	96.67	6.3
0.5	0.46	92.01	4.8
2	2.15	107.5	3.5

Table S3. Comparison of the proposed biosensor with previously reported APE1 detection methods

Method	Principle	LOD (U/mL)	Label-Free	One-Step	Cell Lysate	Ref.
DNA walker +	3D bipedal	0.03	No	No	Yes	[S1]

Method	Principle	LOD (U/mL)	Label-Free	One-Step	Cell Lysate	Ref.
Exo III	DNA walker on AuNP					
Localized Cas12a-CA	Cas12a cascade on AuNP	2.51×10^{-6}	No	Yes	Yes	[S2]
FAC-HCR	Aptamer-based HCR	0.1174	Yes	No	Yes	[S3]
rGO + hairpin probe	rGO adsorption + FAM	0.02	No	Yes	Yes	[S4]
FRET + magnetic beads	FAM/BHQ1 FRET, MB separation	0.03	No	No	Yes	[S5]
Closed cyclic DNA machine	HCR + CHA closed circuit	7.8×10^{-5}	No	No	Yes	[S6]
This work	**N-CQDs + Ag^{+} + APE1-gated poly-T release**	**0.02**	**Yes**	**Yes**	**Yes**	

Note: LOD: limit of detection; U: unit of APE1 activity. “One-Step” indicates whether the entire assay can be performed in a single mixing step without separation or washing. “Cell Lysate” indicates successful detection in complex biological matrices. Detailed information of cited works is provided in the reference list.

Table S4. Intra-day repeatability of the biosensor for 1.0 U/mL APE1 (n = 5).

Replicate	Fluorescence Intensity (a.u)	APE1 Concentration (U/mL)
1	2450	1.02
2	2380	0.98
3	2420	1.00

Replicate	Fluorescence Intensity (a.u)	APE1 Concentration (U/mL)
4	2510	1.05
5	2390	0.99
Mean	2430	1.01
SD	102	0.042
RSD	4.2%	4.2%

Reference

[S1] Liu Q, Zhang Q, Zhang Y, et al. A recognition-induced three-dimensional bipedal DNA walker for highly sensitive detection of APE1. Analytical Methods, 2024, 16(36): 6220-6228.

[S2] Zhang L, Luo S, Fan R, et al. Localized Cas12a-based cascade amplification for sensitive and robust detection of APE1. Talanta, 2024, 280: 126773.

[S3] Liu M, Tan Y, Zhou C, et al. Fluorogenic aptamer-based hybridization chain reaction for signal-amplified imaging of apurinic/apyrimidinic endonuclease 1 in living cells. Biosensors, 2024, 14(6): 274.

[S4] Li F, Xie Q, Qin Y, et al. Real-time monitoring and effector screening of APE1 based on rGO assisted DNA nanoprobe. Analytical biochemistry, 2021, 633: 114394.

[S5] Ren Z, Zhang Q, Wang Y, et al. An “off-on” fluorescent sensor based on FRET and magnetic beads for APE1 activity detection in breast cancer cell lysates. Analytical Methods, 2026, 18(12): 2455-2463.

[S6] Chai Q, Chen J, Zeng S, et al. Closed cyclic DNA machine for sensitive logic operation and APE1 detection. Small, 2023, 19(23): 2207736.